

Supporting Information

Portable microfluidic plasmonic chip for fast real-time cardiac troponin I biomarker thermoplasmonic detection

*Andreea Campu*¹, *Ilinca Muresan*¹, *Monica Potara*¹, *Diana Raluca Lazar*^{2,3}, *Florin-Leontin Lazar*⁴, *Simona Cainap*^{2,5}, *Dan Mircea Olinic*^{4,6}, *Dana Maniu*^{1,7}, *Simion Astilean*^{1,7} and *Monica Focsan*^{1,7*}

¹ Nanobiophotonics and Laser Microspectroscopy Center, Interdisciplinary Research Institute in Bio-Nano-Sciences, Babes-Bolyai University, Treboniu Laurian No. 42, 400271 Cluj-Napoca, Romania.

² Department of Pediatric Cardiology, Pediatric Clinic No. 2, Emergency County Hospital for Children, Crisan No. 3 – 5, 400124 Cluj-Napoca, Romania.

³ 11th Department of Medical Oncology, University of Medicine and Pharmacology “Iuliu Hatieganu”, Republicii No. 34 – 36, 400171 Cluj-Napoca, Romania.

⁴ Department of Interventional Cardiology, Medical Clinic No. 1, Emergency County Hospital, Clinicilor No. 3 – 5, 400006 Cluj-Napoca, Romania.

⁵ Department of Mother & Child, University of Medicine and Pharmacology “Iuliu Hatieganu”, Louis Pasteur No. 4, 400349 Cluj-Napoca, Romania.

⁶ Cardiology Discipline, University of Medicine and Pharmacology “Iuliu Hatieganu”, Louis Pasteur No. 4, 400349 Cluj-Napoca, Romania.

⁷ Biomolecular Physics Department, Faculty of Physics, Babes-Bolyai University, Mihail Kogalniceanu No. 1, 400084 Cluj-Napoca, Romania.

Materials

Tetrachloroauric acid ($\text{HAuCl}_4 \cdot 4\text{H}_2\text{O}$, 99.99%), cetyltrimethylammonium bromide (CTAB, 96%), nitric acid (HNO_3 , 65%), citric acid ($\text{C}_6\text{H}_8\text{O}_7$), cetyltrimethylammonium chloride (CTAC), hydroxyquinoline (HQL, 99%), sodium borohydride (NaBH_4 , 99%), silver nitrate (AgNO_3 , 99%), Phosphate buffered saline (PBS, pH 7.2), glutaraldehyde (GA), Troponin I from human heart (cTnI) and Monoclonal Anti-TNNI3, clone 1E7 antibody produced in mouse, purified immunoglobulin (anti-cTnI), 3-aminopropyltriethoxysilane (APTES, 99%), 4-mercaptobenzoic acid (4-MBA) and para-aminothiophenol (p-ATP) were purchased from Sigma-Aldrich. The glass substrates were acquired from ROTH Karlsruhe (24×50 mm). For the polydimethylsiloxane (PDMS) layers, a Sylgard 182 elastomer kit was obtained from Dow Corning (Midland, USA). All chemicals were used as received. Throughout the experiments, ultrapure water (resistivity ~ 18.2 M Ω) was used as solvent.

Gold nanobipyramids chemical synthesis

Gold nanobipyramids (AuBPs) were synthesized utilizing a previously reported two-step chemical seed-mediated approach [1] adapted from Chateau *et al.* [2]. In brief, in the first step, the gold seeds were prepared by mixing 1 M $\text{HAuCl}_4 \cdot 4\text{H}_2\text{O}$ with 25 w% CTAC, 0.25 M HNO_3 , 50 mM NaBH_4 as reducing agent, and 1 M citric acid under vigorous stirring at room temperature followed by a heat treatment at 85 °C for 90 minutes without stirring. The as-obtained seeds were further used in the second step of the approach, specifically the growth of the AuBPs. Concretely, 18 μL seeds were added to a growth solution comprising 25 mM HAuCl_4 , 0.45 mM CTAB stabilizing agent solution, 30 μl AgNO_3 and 60 μl HQL as reducing agent. The final mixture was thermally treated for 50 minutes at 45 °C. Before use, the reactant excess was removed by applying two purification steps involving the centrifugation of the colloidal AuBPs at 8000 rpm for 15 minutes, extraction of the supernatant and re-dispersion in ultra-pure water.

Characterization Methods

The extinction spectrum of the colloidal AuBPs in solution was recorded using a Jasco V-670 UV-Vis-NIR spectrophotometer with a 2 nm bandwidth and 1 nm spectral resolution. Using a Malvern Instruments Zetasizer Nano ZS90 system, the hydrodynamic diameter of the as-synthesized AuBPs was determined using Dynamic Light Scattering (DLS). The surface charge of the AuBPs was established using the same apparatus to perform Zeta Potential measurements.

The colloidal AuBPs were morphologically characterized using a FEI Tecnai F20 field emission Transmission Electron Microscope (TEM) with an Eagle 4 k CCD camera and 200 kV accelerating voltage. For TEM analysis, the colloid was dropped onto a copper grid coated with a carbon film. The widely available ImageJ tool was used to further examine the acquired TEM microscopic pictures. (ImageJ software, <https://imagej.net/ImageJ>, n.d.). Moreover, after the immobilization of the AuBPs, Scanning Electron Microscopy (SEM) was used to study the surface of the plasmonic nanoplatform using a FEI Quanta 3D FEG dual beam scanning electron microscope operating at a 30 kV accelerating voltage. The plasmonic nanoplatform was sputtered with a 5 nm gold layer using a Q150R ES automated Sputter Coater prior to SEM analysis, which prevented charging, reduced heat damage, and improved the secondary electron signal needed for topographic studies. The morphology of the plasmonic nanoplatform was also investigated by atomic force microscopy (AFM) using a Witec Alpha300A system.

The LSPR spectra of the plasmonic nanoplatform and final chip after each functionalization step and capture of the target cTnI were recorded using a portable Ocean Optics USB 4000 optical UV-Vis spectrophotometer coupled with a ZEISS Axio Observer Z1 system with an inverted optical microscope equipped with a halogen lamp (HAL 100) and a 20× ZEISS objective through an optical fibre having a core diameter of 600 μm.

A portable Raman Systems R3000 CN spectrometer with a 785 nm diode laser, 190 mW laser power and 30 seconds integration time, was used to record the SERS spectra for the evaluation of the SERS sensitivity of the plasmonic nanoplatform. For the SERS detection of the cTnI biomarker in simulated conditions, the confocal Raman microscope Alpha300R Witec was employed. The SERS spectra were acquired under 785 nm laser lines using a 100× objective, 0.9 numeric aperture, a laser power of 8.9 mW and an integration time of 20 seconds per acquisition. The Raman signal

was collected by an optical fibre a diameter of 100 μm and analysed by the UHTS 300 Raman spectrometers equipped with a CCD camera.

For the thermal detection of the cTnI biomarker, the 785 nm laser line of the portable Raman Systems R3000 CN spectrometer was used as excitation, while the laser power was varied from 2.59 to 7.16 W/cm^2 . The thermal maps were recorded every second by a thermographic Optris PI 450 infrared camera with an O38 standard lens and analysed using the corresponding Optris PI software.

Statistical Analysis

The main characteristics of the studied population were analysed using Microsoft Excel 2019. Categorical variables were summarized as frequencies and percentages, and continuous variables as mean \pm standard deviation. The sample distribution parameters were evaluated by Chi-square test. Statistical significance is indicated by two-tail *p-value* less than 0.05. All troponin value was reported as *mean \pm 95% CI* (CI = Confidence Interval).

To assess the quality of the developed microfluidic plasmonic chip, four metrics, which describe the tests' adequacy, were determined, as follows [3]:

The sensitivity of the chip is defined as the probability to obtain a positive test result for a patient, who indeed is suffering from that particular medical condition, and calculated as:

$$Se = \frac{(True\ positive\ value)}{(True\ positive\ value + False\ negative\ value)} \times 100 \quad \text{Equation S1.}$$

On the other hand, the specificity of the chip is the probability to obtain a negative test result for a patient, who is not suffering from that particular medical condition and is determined by:

$$Sp = \frac{(True\ negative\ value)}{(True\ negative\ value + False\ positive\ value)} \times 100 \quad \text{Equation S2.}$$

The positive predictive value (PPV) stands for the probability that a patient with a positive test result indeed suffers from that particular medical condition and is calculated as:

$$PPV = \frac{(True\ positive\ value)}{(True\ positive\ value + False\ positive\ value)} \times 100 \quad \text{Equation S3.}$$

Similarly, the negative predictive value (NPV) stands for the probability that a patient with a negative test result indeed does not suffer from that particular medical condition and is calculated as:

$$NPV = \frac{(True\ negative\ value)}{(True\ negative\ value + False\ negative\ value)} \times 100 \quad \text{Equation S4.}$$

In the equations, the following terms were determined by comparing the test results obtained with the as-developed microfluidic plasmonic chip with clinical determination of troponin's level using the standard ELISA technique – considered the golden standard for the troponin's detection:

True positive value – the patient, who has the disease and the result of the test is positive.

False positive value – the patient does not have the disease, but the test is positive.

True negative value – the patient does not have the disease and the test is negative.

False negative value – the patient has the disease, but the test is negative.

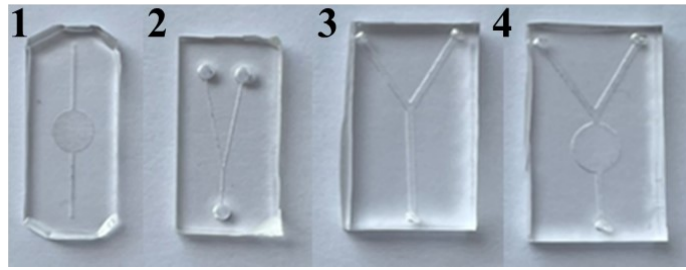


Figure S1. Different microfluidic channel designs realized using an Epilog Zinc 16 Laser Cutter.

Inclusion and Exclusion Criteria for Adult Patients (over 18 years old)

The main inclusion criteria in this study were an established diagnosis commonly associated with elevated cardiac troponin: i) ST elevation myocardial infarction (STEMI); ii) non-ST elevation myocardial infarction (NSTEMI); iii) intermediate-high to high-risk pulmonary embolism; iv) acute heart failure; v) myo-pericarditis; vi) Takotsubo syndrome; vii) post-electrical cardioversion or viii) high-rate tachyarrhythmia.

The main exclusion criteria were: i) pathologies associated with the presence of rheumatoid factor, which could determine cross-reactivity; ii) severe hyper-triglyceridemia or recent intravenous lipid emulsion administration, which could interfere with the serum transparency, causing false positive results; iii) gram **positive** bacterial infections; iv) hemolytic-uremic syndrome or other pathologies which could determine false positive results due to hemolysis, v) severe anaemia and vi) icterus.

Inclusion and Exclusion Criteria for Paediatric Patients (under 18 years old)

The inclusion criteria for paediatric patients were the diagnosis of diseases associated with high serum troponin values, such as: i) myocarditis; ii) pericarditis; iii) Kawasaki disease; iv) congenital heart disease; v) cardiac failure; vi) post-Covid multi-systemic inflammatory disease syndrome.

The main exclusion criteria were i) diseases associated with a positive rheumatoid factor, which could cause cross-reactivity; ii) severe hyper-triglyceridemia or recent intravenous lipid emulsion administration, which could interfere with serum transparency, thus causing false positive results; iii) gram **negative** bacterial infections, iv) hemolytic-uremic syndrome or other hemolysis-associated diseases, which could cause false positive results, v) severe anaemia and vi) icterus.

Main characteristics of the cohort

Table S1. Baseline characteristics of adult and pediatric patients (n (%) – number (percent); sd – standard deviation).

	Adults (n = 50)	p-value	Children (n = 30)	p-value
Sex				
<i>Female n (%)</i>	22 (44)	0.40	13 (43,33)	0.47
<i>Male n (%)</i>	28 (56)		17 (56,67)	
Age (years)				
<i>mean ± sd</i>	55.42 ± 13.79		8.62 ± 2.11	
Risk Factors				
<i>Smoking n (%)</i>	23 (46)	<0.001	COVID-19 infection	<0.001
<i>Diabetes mellitus n (%)</i>	5 (10)			
<i>Chronic kidney disease n (%)</i>	4 (8)			
<i>Unidentified n (%)</i>	18 (36)			

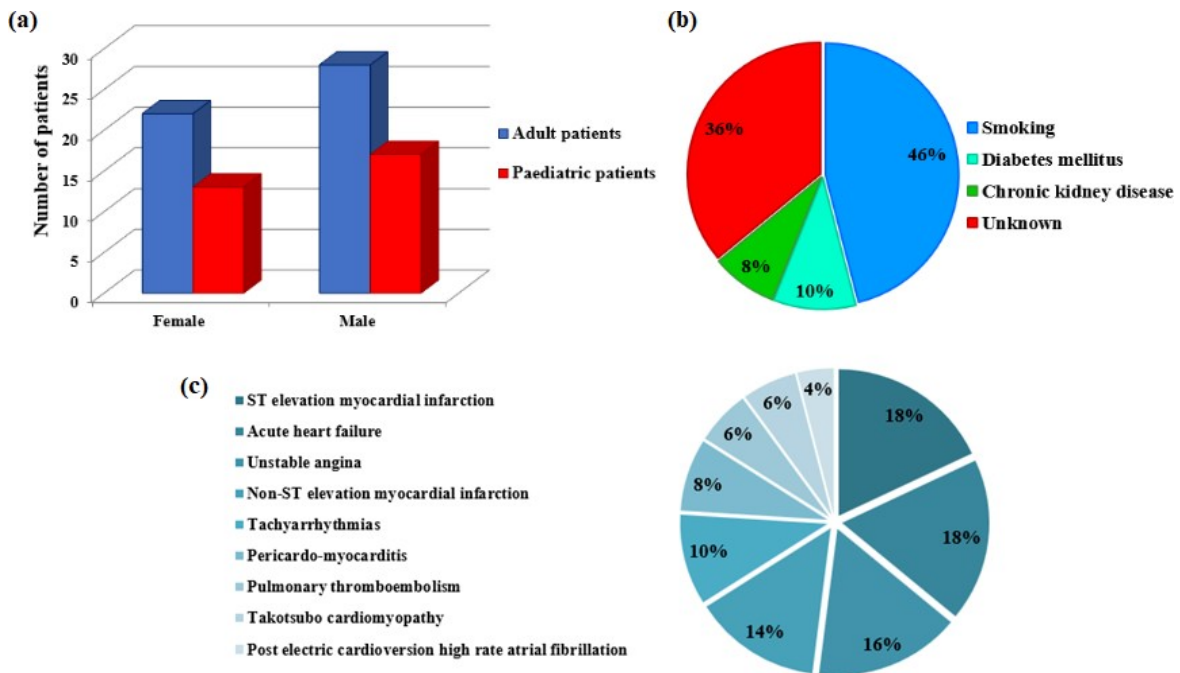


Figure S2. (a) Number of patients according to sex. The distribution of patients on gender does not reveal some statistical relevance ($p\text{-value} > 0.05$) neither in the case of adult patients, nor in the case of pediatric ones. **(b)** Risk factors in adult population. The distribution of identified risk factors for adult patients has high statistical significance ($p\text{-value} < 0.001$). **(c)** Clinical conditions for admission in adult population. No statistical significance ($p\text{-value} > 0.05$) was identified in the distribution of clinical condition in adult population.

Optical and morphological properties of the colloidal nanoparticles

Prior to the immobilization of the AuBPs onto the pre-functionalized glass substrates, the AuBPs were characterized in terms of optical and morphological properties. **Figure S3(a)** presents the extinction spectrum of the as-synthesized AuBPs exhibiting the characteristic optical response of the diamond-like gold nanoparticles consisting of two LSPR bands: one band located at 515 nm arisen due to the transversal oscillations of the electron cloud and an intense band at 830 nm corresponding to the electron oscillations along the longitudinal axis. In the inset of **Fig. S3(a)**, a representative TEM microscopic image is shown proving the bipyramidal shape of the AuBPs as well as their reproducibility in terms of size. Additionally, DLS measurements establish a hydrodynamic diameter of 126 nm (**Fig. S3(b)**), which is supported by the analysis of the TEM images, using the ImageJ toolkit, determining an average length \times width of 115 \times 35 nm (Inset of **Fig. S3(b)**). Furthermore, Zeta Potential measurements revealed a surface charge of + 28 mV (data not shown).

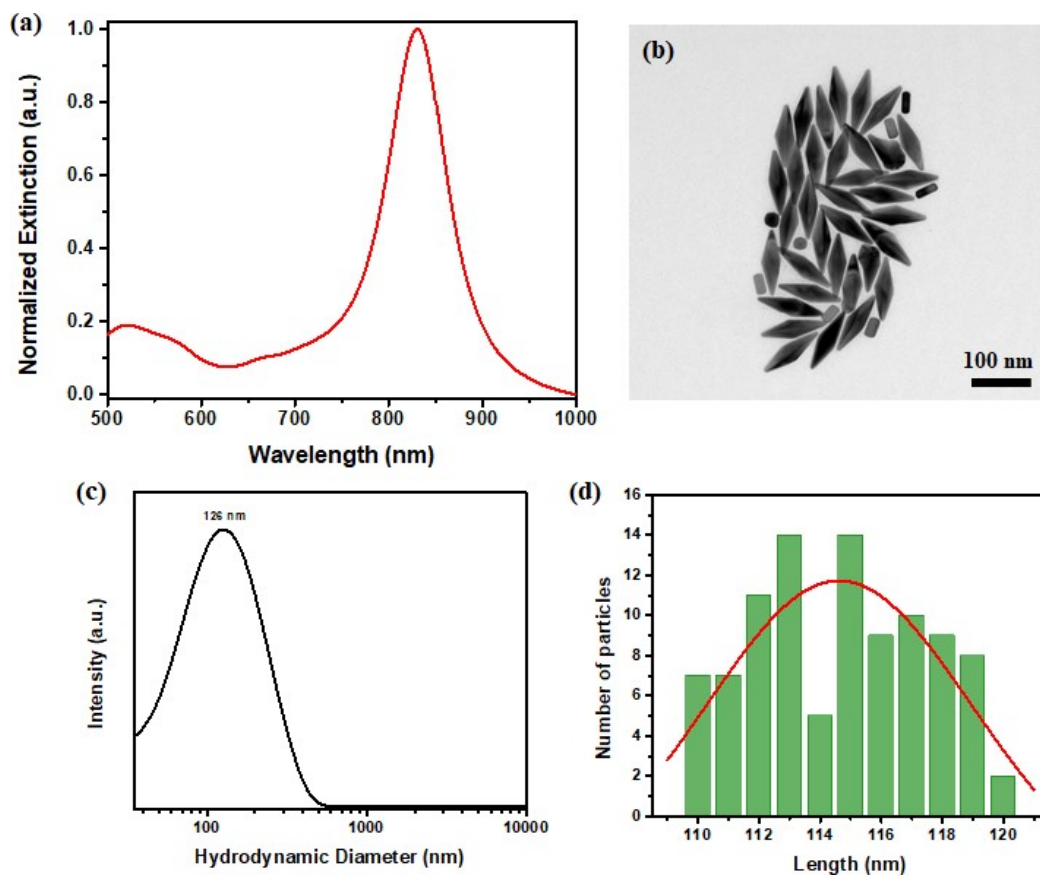


Figure S3. (a) Extinction spectra of the as-synthesized AuBPs in solution. (b) Representative TEM microscopic image of the obtained colloidal AuBPs. (c) DLS measurement to determine the hydrodynamic diameter of the AuBPs. (d) Histogram of the size distribution and Gaussian fitting of the length of 100 nanoparticles based on the TEM image analysis.

Optical and morphological characterization of the plasmonic nanoplatform

In **Fig. S4(a)**, the AuBPs' extinction spectra are presented in comparison before (red spectrum) and after (black spectrum) the immobilization process. The optical response of the AuBPs is well-preserved after being deposited onto the glass substrates, hence the two characteristic LSPR bands are present and well-defined. Moreover, LSPR is highly dependent on the dielectric environment of the nanoparticles, thus, due to the refractive index change from water ($n = 1.333$) to air ($n = 1$), the longitudinal LSPR band is located at 788 nm, 42 nm blue-shifted compared to the longitudinal contribution of the AuBPs in aqueous solution. Moreover, the immobilization process allows the deposition of both individual and self-assembled AuBPs, the latter being confirmed by the appearance of a plasmonic band at higher wavelengths (900 nm) assigned to AuBPs end-to-end assembled chains. SEM (**Fig. S4(b)**) and AFM (**Fig. S4(c)**) are in good agreement with the optical determinations and bring additional proof of the immobilization of both individual as well as AuBPs self-assemblies, thus confirming the successful fabrication of the plasmonic nanoplatform. In terms of sensitivity, a similar substrate was already proven to exhibit high LSPR and SERS sensitivity [4].

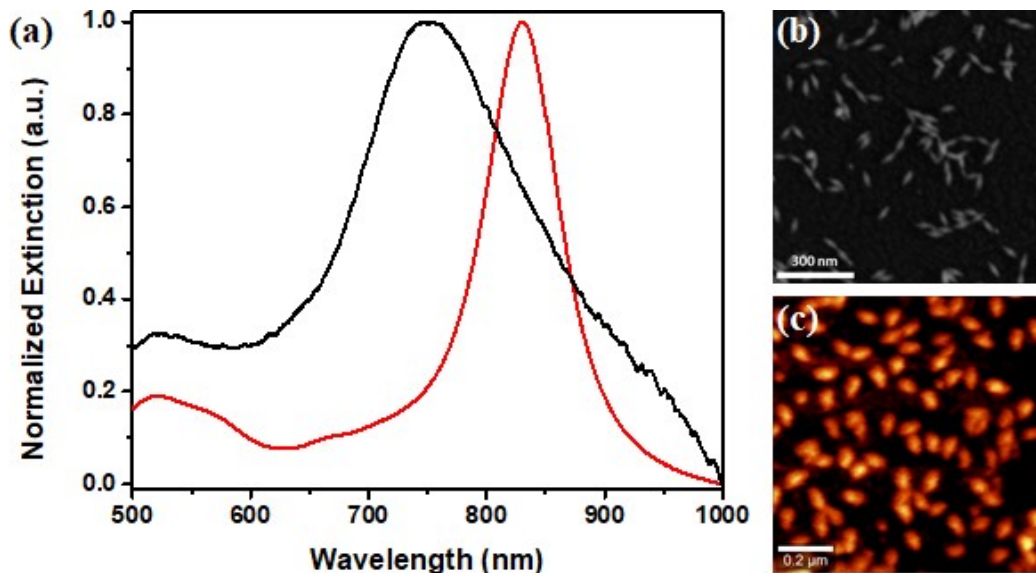


Figure S4. (a) Normalized extinction spectra of the AuBPs in solution (red spectrum) and the fabricated plasmonic nanoplatform (black spectrum). Representative SEM (b) and AFM (c) images of the as-obtained plasmonic nanoplatform.

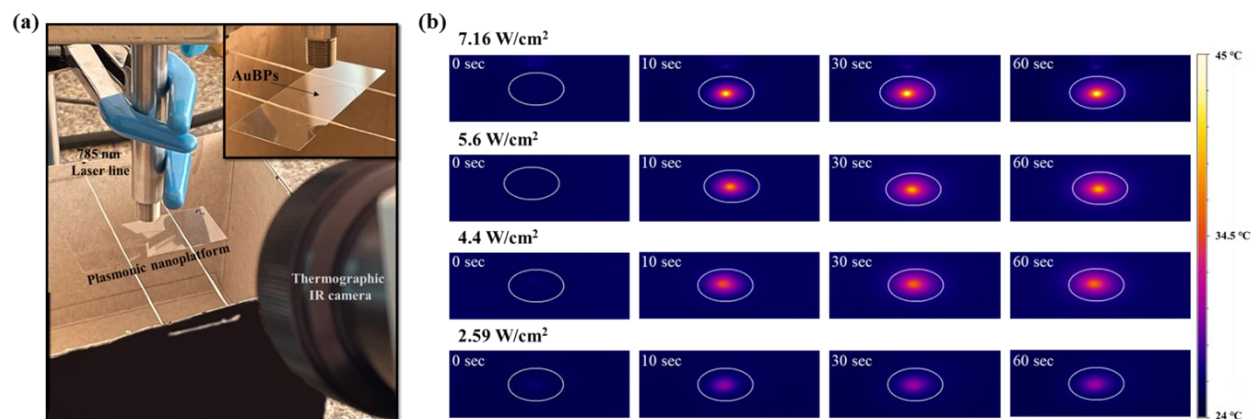


Figure S5. (a) Digital image of the experimental setup for the assessment of the light-to-heat conversion capability of the plasmonic nanoplatform. **(b)** Thermographic images recorded at $t = 0, 10, 30$ and 60 seconds during the exposure of the plasmonic nanoplatform to the 785 nm laser line having different laser power densities.

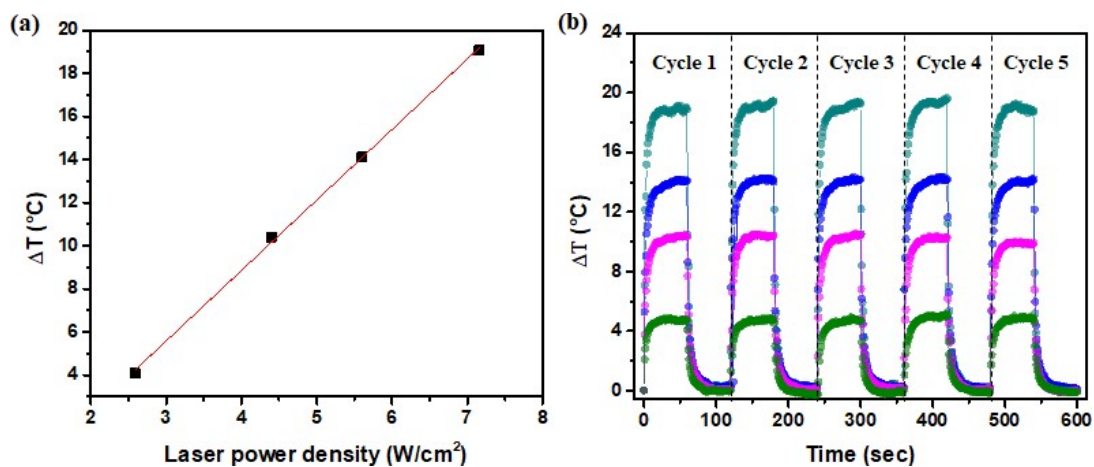


Figure S6. (a) Plot of the calculated temperature difference against the laser power density of the 785 nm excitation laser line. **(b)** The thermal curves after 5 laser ON-OFF cycles of the nanoplatform exposed to 7.16 (cyan spectrum), 5.6 (blue spectrum), 4.4 (magenta spectrum) and 2.59 W/cm² (dark green spectrum) laser power density.

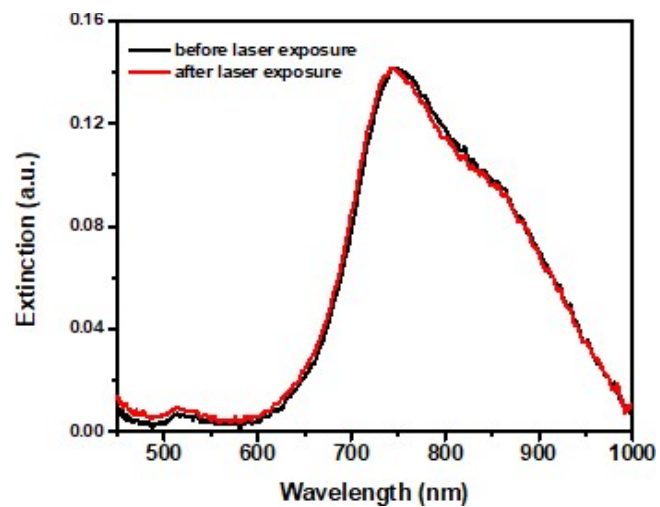


Figure S7. The extinction spectra of the plasmonic substrate before and after the exposure to the 785 nm laser line for 30 seconds.

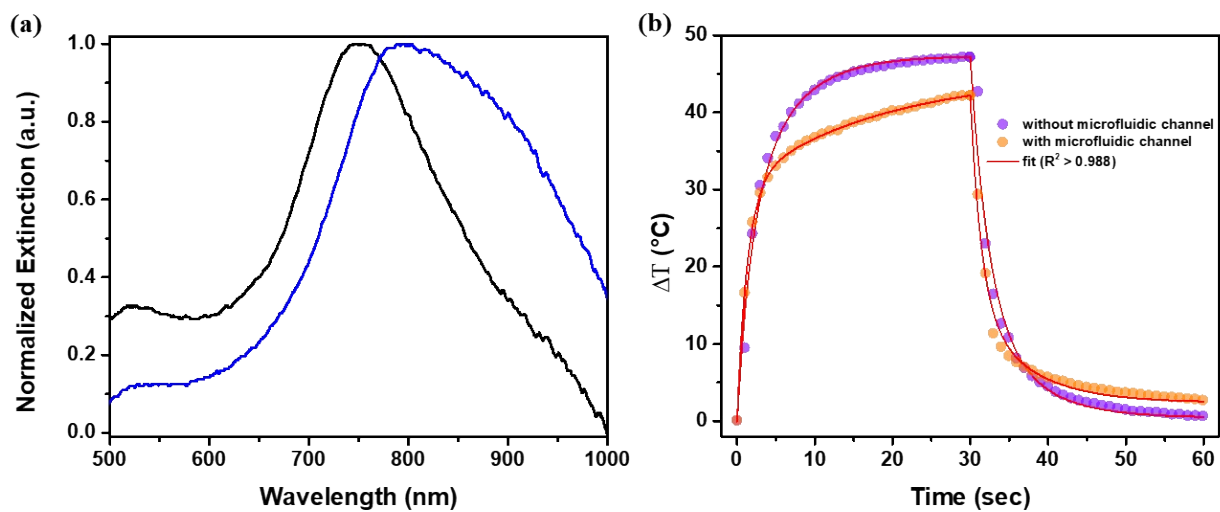


Figure S8. (a) The normalized extinction spectra of the plasmonic nanoplateforms with lower (black spectrum) and higher (blue spectrum) number self-assemblies, (b) The heating and cooling curves obtained for the plasmonic nanoplateform without and with the PDMS microfluidic channel, to investigate the thermal changes induced by the latter.

Analytical determination of the time constant τ_s

The time constant τ_s of the cooling process is described as the slope of the cooling time as a function of the normal logarithm of the temperature driving force, θ , and defined as:

$$\tau_s = \sum m_i C_{p,i} / hA \quad \text{Equation S5.}$$

Where m_i and $C_{p,i}$ represent the masses and specific heats of each component of the investigated system, and h stands for the heat transfer coefficient of the immobilized AuBPs and A is the area cross section of the irradiated surface. θ is expressed as:

$$\theta = \Delta T / (T_{\max} - T_{\text{amb}}) \quad \text{Equation S6.}$$

Determination of the limit of blank (LOB), limit of detection (LOD) and limit of quantification (LOQ)[5-7]

Limit of Blank (LOB)

$$LOB = \text{mean blank} + 1.645 \times \text{standard deviation of blank} \quad \text{Equation S7.}$$

Limit of Detection (LOD)

$$LOD = 3.3 \times \frac{\text{standard deviation of the ordinate intercept}}{\text{slope of the regression line}} \quad \text{Equation S8.}$$

Limit of Quantification (LOQ)

$$LOQ = 10 \times \frac{\text{standard deviation of the ordinate intercept}}{\text{slope of the regression line}} \quad \text{Equation S9.}$$

Computational details

Linear range between 10 – 100 pg/mL:

Equation: $y = 5.53 + 1.37143x$

Slope of the regression line: $Sl = 1.37143$

Standard deviation of the ordinate intercept: $SD = 0.01964$

$R^2 = 0.977$

Linear range between 0.5 – 2 ng/mL:

Equation: $y = 5.94721 + 0.00289x$

Slope of the regression line: $Sl = 0.00289$

Standard deviation of the ordinate intercept: $SD = 0.00368$

$R^2 = 0.999$

Clinical assay of the adult population

For the adult population, most of the patients were admitted for acute coronary syndromes (STEMI – 18 %, NSTEMI – 16 % or unstable angina – 14 %) and acute heart failure (18 %), other diagnosis being illustrated in **Fig. S1(c)** - pathological conditions associated with a significant rise in the cardiac troponins' values. Of note, all patients with Takotsubo cardiomyopathy presented high values of cardiac troponins, electrocardiographic changes and symptoms suggesting acute myocardial infarction, thus the diagnosis was established only after the coronary angiography was performed. The average age of the adult patients was 55.42 ± 3.92 years, with the remark of a significantly lower age of patients with pericardo-myocarditis (32.50 ± 4.68 years). The average time from the onset of symptoms to the time of blood sampling was 4.5 hours, with an average hs-cTnI value of 937.6 ± 322.67 pg/mL. Higher troponin values were recorded in patients with STEMI and pericardo-myocarditis (obtaining an average of 3050 ± 450.34 and 1657 ± 286.81 pg/mL, respectively), while, according to the definition, the samples of patients with unstable angina were within the normal range (below 14 pg/mL). In accordance with the literature, the use of hs-cTn assays in our study resulted in a fast diagnosis of myocardial infarction, as all 32 % of the patients with STEMI/NSTEMI were diagnosed in the first 2 hours from their arrival at the emergency department and less than 4.5 hours from the onset of the symptoms, which was translated in an optimal immediate/early invasive strategy, represented by coronary angiography, followed by percutaneous coronary intervention. This strategy has been demonstrated to reduce the mortality rates in patients with STEMI, as well as in patients with NSTEMI [8]. Moreover, higher values of troponins were detected when the patients have reached the emergency room after a longer period of time from the initial pain episode. Also, the use of hs-cTn allowed the physicians to safely rule-out the diagnosis in 16 % of the cases, which were classified as unstable angina, thus reducing the number of unnecessary emergency coronary angiographies. However, based on the significant rise in the cTn values, associated with significant changes registered on electrocardiogram and echocardiography and corroborated with typical symptoms, 6 % of the patients were classified as acute myocardial infarction and coronary angiography was performed before the diagnosis of Takotsubo cardiomyopathy was established. All patients had a favorable evolution during hospitalization, with early fall in cTnI values after specific medical therapy was initiated. Glaveckaitė *et al.* showed that in-hospital mortality is influenced by the peak concentration of

troponin I [9] and these findings were also validated by our study, as all of the patients had low TnI and natriuretic peptide values.

Another important finding in our study was related to the patients with acute heart failure, in which higher values of troponins were associated with longer hospitalization, the need of higher diuretic doses and lower ejection fraction. In acute heart failure, cTn is released as a response to both non-ischemic (e.g., increased afterload, increased preload, inflammatory signaling, altered calcium handling) and ischemic mechanisms [10] and several studies demonstrated the association between higher troponin values and poorer outcomes during hospitalization and increased risk of death or rehospitalizations during follow-up [11]. Even though the follow-up of these patients was not performed, as it was not relevant for the present study, our findings suggest the importance of troponins as a prognostic and risk factor in patients with acute heart failure, thus a more aggressive medical treatment could improve their short and long-term outcome, as it was suggested by other studies as well [12]. Nevertheless, when assessing the troponin values in patients presenting in the emergency department, it must be taken into consideration that this biomarker can present a significant rise and/or fall in several other cardiac as well as non-cardiac scenarios, such as congenital heart diseases, infective endocarditis, myocarditis, acute pneumonia, atrial fibrillation, intracranial hemorrhage, chronic/acute kidney disease [13] and it should always be interpreted in combination with other biomarkers' changes, clinical and imaging findings. In our study, high troponin values were also found in patients with tachyarrhythmias, post electrical conversion of atrial fibrillation or pericardo-myocarditis. Even though we did not analyze the prognostic value of the biomarker in these settings, several studies have demonstrated high troponin values do not seem to have the same prognostic impact as in acute coronary syndromes [14].

Table S2. Mean troponin level in paediatric patients (pg/mL).

All patients (mean \pm 95% CI)	89.50 \pm 28.02
Boys (mean \pm 95% CI)	98.02 \pm 44.14
Girls (mean \pm 95% CI)	75.30 \pm 22.14

References

- [1] Campu A, Lerouge F, Chateau D, Chaput F, Baldeck P, Parola S, Maniu D, Craciun A M, Vulpoi A, Astilean S and Focsan M 2018 Gold NanoBipyramids Performing as Highly Sensitive Dual-Modal Optical Immunosensors *Anal. Chem.* **90** 8567–75
- [2] Chateau D, Liotta A, Vadcard F, Navarro J R G, Chaput F, Lermé J, Lerouge F and Parola S 2015 From gold nanobipyramids to nanojavelins for a precise tuning of the plasmon resonance to the infrared wavelengths: experimental and theoretical aspects *Nanoscale* **7** 1934–43
- [3] Trevethan R 2017 Sensitivity, Specificity, and Predictive Values: Foundations, Pliabilities, and Pitfalls in Research and Practice *Front. Public Health* **5** 307
- [4] Campu A, Lerouge F, Craciun A-M, Murariu T, Turcu I, Astilean S and Monica F 2020 Microfluidic platform for integrated plasmonic detection in laminal flow *Nanotechnology* **31** 335502
- [5] Armbruster D A and Pry T 2008 Limit of blank, limit of detection and limit of quantitation *Clin Biochem Rev* **29 Suppl 1** S49-52
- [6] Shrivastava A and Gupta V 2011 Methods for the determination of limit of detection and limit of quantitation of the analytical methods *Chron Young Sci* **2** 21
- [7] Natarajan S, DeRosa M C, Shah M I and Jayaraj J 2021 Development and Evaluation of a Quantitative Fluorescent Lateral Flow Immunoassay for Cystatin-C, a Renal Dysfunction Biomarker *Sensors* **21** 3178
- [8] Ottervanger J, Armstrong P, Barnathan E, Boersma E, Cooper J, Ohman E, James S, Wallentin L and Simoons M 2004 Association of revascularisation with low mortality in non-ST elevation acute coronary syndrome, a report from GUSTO IV-ACS *European Heart Journal* **25** 1494–501
- [9] Glaveckaitė S, Šerpytis P, Pečiūraitė D, Purnaitė R and Valevičienė N 2016 Clinical features and three-year outcomes of Takotsubo (stress) cardiomyopathy: Observational data from one center *Hellenic Journal of Cardiology* **57** 428–34
- [10] Harrison N, Favot M and Levy P 2019 The Role of Troponin for Acute Heart Failure *Curr Heart Fail Rep* **16** 21–31
- [11] Diez M, Talavera M L, Conde D G, Campos R, Acosta A and Trivi M S 2016 High-sensitivity troponin is associated with high risk clinical profile and outcome in acute heart failure *Cardiol J.* **23** 78–83
- [12] Lazar D R, Lazar F-L, Homorodean C, Cainap C, Focsan M, Cainap S and Olinic D M 2022 High-Sensitivity Troponin: A Review on Characteristics, Assessment, and Clinical Implications ed N El-Khazragy *Disease Markers* **2022** 1–13

[13] Janardhanan R 2016 Myocarditis with very high troponins: risk stratification by cardiac magnetic resonance *J. Thorac. Dis.* **8** E1333–6

[14] Lombardi C M, Carubelli V, Iorio A, Inciardi R M, Bellasi A, Canale C, Camporotondo R, Catagnano F, Dalla Vecchia L A, Giovinazzo S, Maccagni G, Mapelli M, Margonato D, Monzo L, Nuzzi V, Oriecua C, Peveri G, Pozzi A, Provenzale G, Sarullo F, Tomasoni D, Ameri P, Gnechi M, Leonardi S, Merlo M, Agostoni P, Carugo S, Danzi G B, Guazzi M, La Rovere M T, Mortara A, Piepoli M, Porto I, Sinagra G, Volterrani M, Specchia C, Metra M and Senni M 2020 Association of Troponin Levels With Mortality in Italian Patients Hospitalized With Coronavirus Disease 2019: Results of a Multicenter Study *JAMA Cardiol* **5** 1274